Efficient spectral domain technique for the frequency locking analysis of nonlinear oscillators

EPJ manuscript No.
(will be inserted by the editor)

Efficient spectral domain technique for the frequency locking analysis of nonlinear oscillators

M. Bonnin[1], F.L. Traversa[2], and F. Bonani[1]

[1] Dipartimento di Elettronica e Telecomunicazioni, Politecnico di Torino
[2] MemComputing, San Diego, USA

the date of receipt and acceptance should be inserted later

Abstract. After discussing an implementation of the Harmonic Balance technique that enables the efficient determination of the limit cycles for a nonlinear autonomous dynamical system, we consider the frequency locking of a set of oscillators that is studied by means of a proper extension of the aforementioned approach. Harmonic Balance is also used for the numerical computation of the Floquet exponents and eigenvectors of the frequency locked limit cycle, thus enabling the assessment of its stability properties. The proposed technique is applied to the study of the frequency locking properties of a set of coupled Chua's oscillators as a function of several parameters.

PACS. 05.45.Xt Synchronization; coupled oscillators – 02.60.Lj Differential equations, numerical approximation and analysis – 02.70.Hm Spectral methods

1 Introduction

Synchronization processes in populations of locally interacting elements are a classical problem in nonlinear dynamics, having attracted the attention of researchers from different areas as physics, biology, chemistry, engineering and social sciences [1, 2]. Biological examples include pacemaker cells in the heart [3] and circadian pacemaker cells in the supra chiasmatic nucleus of the brain [4]. Examples taken from physics and engineering includes synchronization of laser arrays [5, 6], microwave oscillators [7], and cellular neural networks (CNN) [8].

Synchronization of neural oscillators plays also a prominent role in the social activities of human beings. It has been shown that synchronization is related to the highest cognitive tasks performed by groups of individuals. For example, the effect of synchrony has been described in experiments of people communicating, or working together with a background of shared, non-directive conversation, song or rhythm, or of groups of children interacting to an unconscious beat. Common rhythm strengthen the group bond, while the lack of such synchrony can indicate unconscious tension, when goals cannot be identified nor worked towards because the members are "out of sync" [9].

When an enormous system of identical or nearly identical oscillators are connected together to form a network, they may spontaneously lock to a common frequency, despite the unavoidable differences in the natural frequencies of the uncoupled oscillators, with a fixed phase difference between them [10]. The simplest patterns are in–phase and anti–phase locking, that occur when all the oscillators share the same phase, or when adjacent oscillators have opposite phases, respectively. Other common patterns are waves propagation, typically solitary waves in one dimension, spiral waves in two dimensions and scroll waves in three dimensional systems [11–13].

At the opposite end of the spectrum is incoherence. When the variance of natural frequencies is large compared to the coupling, the phases of all the oscillators drift quasi periodically with respect to each other, and the system shows no spatial structure whatsoever.

These coherent structures are the result of two competing mechanisms: on the one hand differences in the natural frequencies of the oscillators are disruptive to synchronization, on the other hand couplings between the oscillator favor the formation of coherent patterns. If the variance of the frequency distribution is large, the oscillators run incoherently, each one near its natural frequency, and the phases of the oscillators drift apart. This behavior persists when increasing the coupling strength between the oscillators, until a certain threshold is reached. The threshold level depends on the frequency mismatch, i.e. the frequency difference, between the oscillators: the higher the mismatch, the larger the threshold. Above threshold the oscillators begin to synchronize spontaneously, forming pools of frequency locked oscillators, with constant phase differences. These ensembles of locked oscillators can coexist with ensemble of unlocked ones, the latter belonging to the tails of the frequency distribution. Increasing further the coupling strength

may induce different ensembles to lock to a common state, where in the time one ensemble takes to make m oscillations, the other makes n oscillations, with m and n natural numbers. This type of $m : n$ resonance is an example of frequency locking without phase locking.

Frequency locked states correspond to periodic oscillations in the full dynamical model. Therefore, the research of frequency locked oscillations can be reduced to determine the existence of limit cycles, their number and their stability in the network. Time domain numerical simulations are a valuable tool for this kind of analysis, but may become unfeasible in reasonable computation time for networks composed by a large number of oscillators of high order. Moreover, simulations should be performed for all sets of initial conditions, to determine the total number of limit cycles, their stability and basins of attraction, and for all values of the parameters, to identify the main bifurcation phenomena. Finally, it should be noted that while completely unstable limit cycles can be identified and analyzed performing numerical simulations backward in time, saddle type limit cycles, i.e. periodic solutions that have both stable and unstable manifolds, cannot be detected by time-domain numerical simulations. Numerical techniques such as shooting method and recurrence plots, e.g. Poincaré map and others, have similar limitations.

Engineering oriented, frequency domain techniques, have been recently used to study the dynamic behavior of space–invariant dynamic arrays [14–17]. The main advantages of frequency domain spectral techniques, like the the Harmonic Balance (HB) approach, is that they are able to detect both stable and unstable limit cycle. Furthermore, they do not follow the transient, finding immediately the steady state solutions. In [18] a mixed time–frequency domain method was developed, to detect and characterize limit cycles of nonlinear oscillators. The method was based on the application of the HB technique to find the limit cycle, and on a time domain numerical technique for the calculation of Floquet's multipliers, to determine the stability of the periodic solution. In [19], the authors developed a HB based technique for the analysis of nonlinear oscillators described by differential algebraic equations. The strength of the method lies in the use for the stability analysis, of the same Jacobian matrix of the nonlinear system used in the Newton iterative numerical solution of the HB equations.

In this contribution we propose a frequency–domain numerical technique based on the Harmonic Balance approach implemented according to [8, 19]. In particular the proposed technique is based on:

1. the determination of the frequency locked states (both stable and unstable) through an efficient implementation of the Harmonic Balance technique. Efficiency is attained by means of a numerical estimation of the Fourier coefficients for the nonlinear functions based on a collocation technique that avoids the explicit computation of the Fourier integrals. A side effect of this efficient approach is the possibility to use a large number of harmonics to describe the limit cycle, thus guaranteeing a high accuracy;
2. the use of a general numerical technique that allows for the accurate computation of the Floquet exponents which is based on the same matrices exploited in the implementation of the previous step.

We show the effectiveness of the proposed approach by studying the frequency locking of a network of nonlinear oscillators.

2 Problem statement

Nonlinear oscillators can be conveniently modeled exploiting differential equations that describe the time evolution for state variables of the oscillators. Mathematical models can be made more accurate including different physical effects. For instance, time delays can be taken into account, modeling time lags in the interactions with finite range and finite propagation speed. However, accuracy comes at a price: inclusion of delays in the differential equation requires the full machinery of functional differential equations (FDEs) [20]. Spectral methods such as harmonic balance have been successfully applied to systems with delay [21] and to systems with memory [22]. However, FDEs "evolve" in an infinite dimensional functional space, and the stability of the synchronous oscillations should be assessed using generalized Floquet's multipliers [23, 24]. This is still work in progress from our part, due to the non trivial numerical determination of the generalized Floquet quantities.

Another important related issue is the role that noise plays in synchronization phenomena [25, 26]. As a matter of fact real world oscillators are subject to different noise disturbances, both internal and external. As a consequence they are best described in terms of stochastic differential equations (SDEs) [27]. In presence of noise, trajectories are not periodic any longer, thus strictly speaking harmonic balance cannot be used for noisy nonlinear systems. However, HB has been successfully applied in combination with perturbation techniques for the analysis of noise effects in nonlinear oscillators, both at the single level and for networks. In [28, 29] the authors used a Harmonic Balance technique to determine the limit cycle of a noiseless oscillator, and then a perturbation method to derive a phase deviation equation for the noisy oscillator. A similar approach was used in [30], where the authors considered a network of oscillators with noisy interactions. The stability analysis of noisy nonlinear oscillators is a major problem. In fact stability (and bifurcations) of stochastic systems can be assessed only in a probabilistic sense, by studying qualitative changes in the stationary probability density function of the associated Fokker-Planck equation.

For the sake of simplicity, we shall consider a set of n oscillators, each represented by a size m dynamical system that we will assume to take the form of an ODE system:

$$\dot{\mathbf{x}}_i = \mathbf{f}_i(\mathbf{x}_i) \qquad i = 1, \ldots, n \tag{1}$$

An asymptotic limit cycle of (1) is an isolated periodic solution $\mathbf{x}_{i0}(t)$, characterized by period T_i and angular frequency $\omega_i = 2\pi/T_i$.

The coupled system of n oscillators takes the compact form

$$\dot{\mathbf{x}} = \mathbf{f}(\mathbf{x}) + \epsilon \mathbf{g}(\mathbf{x}) \tag{2}$$

where ϵ is a scalar parameter measuring the coupling strength, and

$$\mathbf{x} = \begin{bmatrix} \mathbf{x}_1 \\ \vdots \\ \mathbf{x}_n \end{bmatrix} \qquad \mathbf{f}(\mathbf{x}) = \begin{bmatrix} \mathbf{f}_1(\mathbf{x}_1) \\ \vdots \\ \mathbf{f}_n(\mathbf{x}_n) \end{bmatrix} \qquad \mathbf{g}(\mathbf{x}) = \begin{bmatrix} \mathbf{g}_1(\mathbf{x}) \\ \vdots \\ \mathbf{g}_n(\mathbf{x}) \end{bmatrix} \tag{3}$$

Frequency locking among the oscillators corresponds to a limit cycle of the full system (2) with period $T(\epsilon)$ and angular frequency $\omega(\epsilon) = 2\pi/T(\epsilon)$. Of course for $\epsilon \to 0$ the coupled systems decouples in the collection of the independent oscillators.

The stability of the limit cycle can be assessed in the following way. If we assume that the solution $\mathbf{x}_0(t)$ is slightly perturbed by a small variation $\delta\mathbf{x}$ such that in (2) $\mathbf{x} = \mathbf{x}_0 + \delta\mathbf{x}$, the perturbation satisfies the linearization of (2) around the solution $\mathbf{x}_0$:

$$\delta\dot{\mathbf{x}} = \mathbf{J}_{\mathbf{f}+\mathbf{g}}(\mathbf{x}_0)\delta\mathbf{x} \tag{4}$$

where

$$\mathbf{J}_{\mathbf{f}+\mathbf{g}}(\mathbf{x}_0) = \mathbf{J}_{\mathbf{f}}(\mathbf{x}_0) + \epsilon \mathbf{J}_{\mathbf{g}}(\mathbf{x}_0) \tag{5}$$

$\mathbf{J}_{\mathbf{f}}$ and $\mathbf{J}_{\mathbf{g}}$ being the Jacobian matrices of the nonlinear functions $\mathbf{f}$ and $\mathbf{g}$, respectively. Since the limit cycle $\mathbf{x}_0(t)$ is periodic, the same property applies to the Jacobian matrices and therefore the solution of (4), following Floquet theorem [31,32], takes the form

$$\delta\mathbf{x}(t) = \mathbf{u}_k(t)\, \mathrm{e}^{\mu_k t} \qquad k = 1, \ldots, mn \tag{6}$$

where μ_k is the Floquet exponent (FE) for the limit cycle, and $\mathbf{u}_k^{(n)}(t)$ is the corresponding Floquet (direct) eigenvector. Direct substitution of (6) into (4) leads to the following eigenvalue problem

$$\dot{\mathbf{u}}_k + \mu_k \mathbf{u}_k = \mathbf{J}_{\mathbf{f}+\mathbf{g}}(\mathbf{x}_0)\mathbf{u}_k \tag{7}$$

that defines the Floquet quantities characterizing the stability of the frequency locked limit cycle.

3 Harmonic Balance determination of the frequency locked limit cycle

We propose here a numerical technique for the accurate determination of the frequency locked limit cycle $\mathbf{x}_0(t)$ based on an efficient implementation of the Harmonic Balance (HB) technique [19,33,34] that makes use of a large number of harmonics in the approximation of the periodic functions exploiting Fourier series.

3.1 The principle of HB: a simple scalar example

Let us consider first a scalar nonlinear, non autonomous ODE containing a nonlinear term and a time-periodic forcing signal $g(t)$

$$\frac{\mathrm{d}x}{\mathrm{d}t} = f(x) + g(t) \tag{8}$$

where $x(t)$ is the unknown function, $f(x)$ is a scalar nonlinear function and $g(t)$ is a T-periodic forcing term. We assume that (8) admits of a limit cycle $x_{\mathrm{S}}(t)$ with period T and angular frequency $\omega = 2\pi/T$.

HB transforms the differential problem (8) into an algebraic system having as unknowns the Fourier coefficients of $x_{\mathrm{S}}(t)$. In fact, $x_{\mathrm{S}}(t)$ can be developed in Fourier series that, for the numerical implementation, needs to be truncated to a finite number of terms N_{H}, the result of a trade-off between accuracy (large N_{H}), and numerical efficiency:

$$x_{\mathrm{S}}(t) = \tilde{x}_{\mathrm{S},0}^{(\mathrm{c})} + \sum_{h=1}^{N_{\mathrm{H}}} \left[\tilde{x}_{\mathrm{S},h}^{(\mathrm{c})} \cos(h\omega t) + \tilde{x}_{\mathrm{S},h}^{(\mathrm{s})} \sin(h\omega t) \right], \tag{9}$$

where $\tilde{x}_{\mathrm{S},h}^{(\mathrm{c})}$ and $\tilde{x}_{\mathrm{S},h}^{(\mathrm{s})}$ are the Fourier coefficients of the (trigonometric) series.

A numerically efficient evaluation of the harmonic coefficients [33, 34] is carried out as follows: since we represent $x_{\mathrm{S}}(t)$ with $2N_{\mathrm{H}}+1$ real coefficients, $2N_{\mathrm{H}}+1$ time samples $t_h = hT/(2N_{\mathrm{H}}+1)$ $(h = 1, \ldots, 2N_{\mathrm{H}}+1)$, equally spaced into the period $]0, T]$, are chosen. Correspondingly, we define an invertible linear operator $\mathbf{\Gamma}$ allowing for the time-frequency transformation [34] between the vector $\hat{\mathbf{x}}_{\mathrm{S}} = [x_{\mathrm{S}}(t_1), \ldots, x_{\mathrm{S}}(t_{2N_{\mathrm{H}}+1})]^{\mathrm{T}}$ ($^{\mathrm{T}}$ represents the transpose) collecting the time samples, and the vector of harmonic amplitudes $\tilde{\mathbf{x}}_{\mathrm{S}} = [\tilde{x}_{\mathrm{S},0}^{(\mathrm{c})}, \tilde{x}_{\mathrm{S},1}^{(\mathrm{c})}, \tilde{x}_{\mathrm{S},1}^{(\mathrm{s})}, \ldots, \tilde{x}_{\mathrm{S},N_{\mathrm{H}}}^{(\mathrm{c})}, \tilde{x}_{\mathrm{S},N_{\mathrm{H}}}^{(\mathrm{c})}]^{\mathrm{T}}$

$$\tilde{\mathbf{x}}_{\mathrm{S}} = \mathbf{\Gamma}\hat{\mathbf{x}}_{\mathrm{S}} \Longleftrightarrow \hat{\mathbf{x}}_{\mathrm{S}} = \mathbf{\Gamma}^{-1}\tilde{\mathbf{x}}_{\mathrm{S}}. \tag{10}$$

The formal expression of the transformation is provided in (11), although for numerical efficiency it is (together with the inverse operator) implemented according to the Discrete Fourier Transform (DFT) algorithm.

$$\mathbf{\Gamma}^{-1} = \begin{bmatrix} 1 & \gamma_{1,1}^{\mathrm{c}} & \gamma_{1,1}^{\mathrm{s}} & \cdots & \gamma_{1,N_{\mathrm{H}}}^{\mathrm{c}} & \gamma_{1,N_{\mathrm{H}}}^{\mathrm{s}} \\ 1 & \gamma_{2,1}^{\mathrm{c}} & \gamma_{2,1}^{\mathrm{s}} & \cdots & \gamma_{2,N_{\mathrm{H}}}^{\mathrm{c}} & \gamma_{2,N_{\mathrm{H}}}^{\mathrm{s}} \\ \vdots & \vdots & \vdots & & \vdots & \vdots \\ 1 & \gamma_{2N_{\mathrm{H}}+1,1}^{\mathrm{c}} & \gamma_{2N_{\mathrm{H}}+1,1}^{\mathrm{s}} & \cdots & \gamma_{2N_{\mathrm{H}}+1,N_{\mathrm{H}}}^{\mathrm{c}} & \gamma_{2N_{\mathrm{H}}+1,N_{\mathrm{H}}}^{\mathrm{s}} \end{bmatrix} \tag{11}$$

where

$$\gamma_{p,q}^{\mathrm{c}} = \cos(q\omega t_p) = \cos\left(\frac{q2\pi p}{2N_{\mathrm{H}}+1}\right), \qquad \gamma_{p,q}^{\mathrm{s}} = \sin(q\omega t_p) = \sin\left(\frac{q2\pi p}{2N_{\mathrm{H}}+1}\right). \tag{12}$$

Because of the chosen time samples, operator $\mathbf{\Gamma}$ is independent of ω, a property exploited when the limit cycle of an autonomous systems is sought for [34] (see Sec. 3.2), since in that case the oscillation frequency ω is one of the problem unknowns.

A direct computation shows that

$$\tilde{\dot{\mathbf{x}}}_{\mathrm{S}} = \mathbf{\Gamma}\hat{\dot{\mathbf{x}}}_{\mathrm{S}} = \omega\mathbf{\Omega}\tilde{\mathbf{x}}_{\mathrm{S}} \tag{13}$$

where $\omega\mathbf{\Omega}$ is the representation of the derivative operator in the Fourier domain

$$\mathbf{\Omega} = \begin{bmatrix} 0 & 0 & 0 & 0 & 0 \ldots & 0 & 0 \\ 0 & 0 & 1 & 0 & 0 \ldots & 0 & 0 \\ 0 & -1 & 0 & 0 & 0 \ldots & 0 & 0 \\ 0 & 0 & 0 & 0 & 2 \ldots & 0 & 0 \\ 0 & 0 & 0 & -2 & 0 \ldots & 0 & 0 \\ \vdots & \vdots & \vdots & \vdots & \vdots & \vdots & \vdots \\ 0 & 0 & 0 & 0 & 0 \ldots & 0 & N_{\mathrm{H}} \\ 0 & 0 & 0 & 0 & 0 \ldots & -N_{\mathrm{H}} & 0 \end{bmatrix}. \tag{14}$$

Finally, we represent in the Fourier domain the nonlinear function $y_{\mathrm{S}}(t) = f(x_{\mathrm{S}}(t))$. Denoting as $\hat{\mathbf{f}}$ the time samples of $f(x_{\mathrm{S}}(t))$, we find

$$\tilde{\mathbf{y}}_{\mathrm{S}} = \mathbf{\Gamma}\hat{\mathbf{y}}_{\mathrm{S}} = \mathbf{\Gamma}\hat{\mathbf{f}}(\hat{\mathbf{x}}_{\mathrm{S}}) = \mathbf{\Gamma}\hat{\mathbf{f}}(\mathbf{\Gamma}^{-1}\tilde{\mathbf{x}}_{\mathrm{S}}) \tag{15}$$

and similarly for $g(t)$, which however is independent of the unknown limit cycle.

Combining (10) and (15), we can convert the sampled version of (8) into an algebraic system of $2N_{\mathrm{H}}+1$ real equations in the $2N_{\mathrm{H}}+1$ real unknowns $\tilde{\mathbf{x}}_{\mathrm{S}}$:

$$\omega\mathbf{\Omega}\tilde{\mathbf{x}}_{\mathrm{S}} = \mathbf{\Gamma}\hat{\mathbf{f}}(\mathbf{\Gamma}^{-1}\tilde{\mathbf{x}}_{\mathrm{S}}) + \mathbf{\Gamma}\hat{\mathbf{g}}. \tag{16}$$

The numerical solution of (16) is normally carried out applying the Newton approach [33], which in turn requires the availability of the Jacobian matrix of all of the nonlinear functions.

It is worth mentioning that in the implementation all the multiplications involving $\mathbf{\Gamma}$ and $\mathbf{\Gamma}^{-1}$ are actually efficiently handled using the Fast Fourier Transform (FFT) algorithm [35]. However, we retain here the $\mathbf{\Gamma}$ formalism rather than the explicit use of the FFT since it makes easier the manipulation of the HB equations.

3.2 The autonomous case: oscillator HB analysis

Let us consider now the case of a vector nonlinear oscillator, e.g. the i-th oscillator of the set represented by (1) for fixed i. We can extend the formulation in Sec. 3.1 as follows. Let $x_{i0,k}(t)$ be the k-th element of the solution $\mathbf{x}_{i0}(t)$.

We define the sample vectors (of size $m(2N_\mathrm{H}+1)$)

$$\hat{\mathbf{x}}_{i0} = \begin{bmatrix} \hat{\mathbf{x}}_{i0,1} \\ \vdots \\ \hat{\mathbf{x}}_{i0,m} \end{bmatrix} \qquad \tilde{\mathbf{x}}_{i0} = \begin{bmatrix} \tilde{\mathbf{x}}_{i0,1} \\ \vdots \\ \tilde{\mathbf{x}}_{i0,m} \end{bmatrix} \tag{17}$$

The time-frequency transformation formally becomes

$$\tilde{\mathbf{x}}_{i0} = \boldsymbol{\Gamma}_m \hat{\mathbf{x}}_{i0} \Longleftrightarrow \hat{\mathbf{x}}_{i0} = \boldsymbol{\Gamma}_m^{-1} \tilde{\mathbf{x}}_{i0} \tag{18}$$

where

$$\boldsymbol{\Gamma}_m = \mathrm{diag}\{\overbrace{\boldsymbol{\Gamma}, \ldots, \boldsymbol{\Gamma}}^{m \text{ times}}\} \tag{19}$$

is a block diagonal matrix of size $m(2N_\mathrm{H}+1) \times m(2N_\mathrm{H}+1)$.

Similarly, for the time derivative operator we find

$$\dot{\tilde{\mathbf{x}}}_{i0} = \boldsymbol{\Gamma}_m \dot{\hat{\mathbf{x}}}_{i0} = \omega_i \boldsymbol{\Omega}_m \tilde{\mathbf{x}}_{i0} \tag{20}$$

where

$$\boldsymbol{\Omega}_m = \mathrm{diag}\{\overbrace{\boldsymbol{\Omega}, \ldots, \boldsymbol{\Omega}}^{m \text{ times}}\}. \tag{21}$$

In the vector case, we need also to express in the frequency domain the matrix-vector product. We consider $\boldsymbol{\beta}(t) = \mathbf{L}(t)\boldsymbol{\alpha}(t)$, where $\mathbf{L}(t)$ is a matrix (of size $p \times q$) made of elements $L_{m,n}(t)$ that are either constant or T_i-periodic. The time-sampled version of $\mathbf{L}(t)$ is a matrix $\hat{\mathbf{L}}$ of size $p(2N_\mathrm{H}+1) \times q(2N_\mathrm{H}+1)$ built expanding each element $L_{k_1,k_2}(t)$ into a diagonal matrix $\hat{\mathbf{L}}_{k_1,k_2}$ of size $(2N_\mathrm{H}+1) \times (2N_\mathrm{H}+1)$ made of the time samples of $L_{k_1,k_2}(t)$. Therefore

$$\tilde{\boldsymbol{\beta}} = \boldsymbol{\Gamma}_p \hat{\mathbf{L}} \hat{\boldsymbol{\alpha}} = \boldsymbol{\Gamma}_p \hat{\mathbf{L}} \boldsymbol{\Gamma}_q^{-1} \tilde{\boldsymbol{\alpha}} = \tilde{\mathbf{L}} \tilde{\boldsymbol{\alpha}} \tag{22}$$

where $\tilde{\mathbf{L}} = \boldsymbol{\Gamma}_p \hat{\mathbf{L}} \boldsymbol{\Gamma}_q^{-1}$. It can be noticed that, while $\hat{\mathbf{L}}_{k_1,k_2}$ is a diagonal matrix, the correspondent block $\tilde{\mathbf{L}}_{k_1,k_2} = \boldsymbol{\Gamma} \hat{\mathbf{L}}_{k_1,k_2} \boldsymbol{\Gamma}^{-1}$ of $\tilde{\mathbf{L}}$ is no longer necessarily a diagonal matrix (it is iff $L_{k_1,k_2}(t)$ is constant) but a full matrix.

Time-sampling and frequency-transforming the governing equation (1) for each of the decoupled oscillators, we find the vector generalization of (16). However, in this case the forcing term is zero (i.e., $\hat{\mathbf{g}} = \mathbf{0}$), and ω_i is a problem unknown as well as $\tilde{\mathbf{x}}_{i0}$, thus raising the number of unknowns to $m(2N_\mathrm{H}+1)+1$. Since the number of equations found from (1) is $m(2N_\mathrm{H}+1)$, we need a further independent equation to close the system. The latter is provided exploiting the fact that the time reference for an autonomous system is not fixed, thus making it possible to nail the phase of one of the solution harmonics without any loss of information. The usual approach consists of setting to zero one of the (non DC component) harmonic amplitudes, thus leading to the nonlinear algebraic system of $m(2N_\mathrm{H}+1)+1$ equations in the $m(2N_\mathrm{H}+1)+1$ unknowns $(\omega_i, \tilde{\mathbf{x}}_{i0})$:

$$\begin{cases} \omega_i \boldsymbol{\Omega}_m \tilde{\mathbf{x}}_{i0} - \boldsymbol{\Gamma}_m \hat{\mathbf{f}}_i(\boldsymbol{\Gamma}_m^{-1} \tilde{\mathbf{x}}_{i0}) = \mathbf{0} \\ \mathbf{P}_{1i}^\mathrm{T} \tilde{\mathbf{x}}_{i0} = 0 \end{cases} \tag{23}$$

where $\mathbf{P}_{1i}^\mathrm{T}$ is a row vector of size $m(2N_\mathrm{H}+1)$ with zero elements apart from a 1 in the position corresponding to the spectral coefficient set to zero to close the HB system.

3.3 The coupled oscillators case

Time sampling and frequency transformation of (2) leads to the full HB nonlinear system of $nm(2N_\mathrm{H}+1)+1$ equations in the $nm(2N_\mathrm{H}+1)+1$ unknowns $(\omega, \tilde{\mathbf{x}})$

$$\begin{cases} \omega \boldsymbol{\Omega}_{nm} \tilde{\mathbf{x}}_0^{(n)} - \begin{bmatrix} \boldsymbol{\Gamma}_m \hat{\mathbf{f}}_1(\boldsymbol{\Gamma}_m^{\text{-}1} \tilde{\mathbf{x}}_{10}) \\ \vdots \\ \boldsymbol{\Gamma}_m \hat{\mathbf{f}}_m(\boldsymbol{\Gamma}_m^{\text{-}1} \tilde{\mathbf{x}}_{m0}) \end{bmatrix} - \epsilon \begin{bmatrix} \boldsymbol{\Gamma}_m \hat{\mathbf{g}}_1(\boldsymbol{\Gamma}_{nm}^{\text{-}1} \tilde{\mathbf{x}}_0^{(n)}) \\ \vdots \\ \boldsymbol{\Gamma}_m \hat{\mathbf{g}}_m(\boldsymbol{\Gamma}_{nm}^{\text{-}1} \tilde{\mathbf{x}}_0^{(n)}) \end{bmatrix} = \mathbf{0} \\ \mathbf{P}_{1,n}^\mathrm{T} \tilde{\mathbf{x}}_0^{(n)} = 0 \end{cases} \tag{24}$$

where we have defined the augmented matrices (size $[nm(2N_{\mathrm{H}}+1)] \times [nm(2N_{\mathrm{H}}+1)]$)

$$\mathbf{\Gamma}_{nm} = \mathrm{diag}\{\overbrace{\mathbf{\Gamma}_m, \ldots, \mathbf{\Gamma}_m}^{n \text{ times}}\} \qquad \mathbf{\Omega}_{nm} = \mathrm{diag}\{\overbrace{\mathbf{\Omega}_m, \ldots, \mathbf{\Omega}_m}^{n \text{ times}}\} \tag{25}$$

and the augmented vector (size $1 \times [nm(2N_{\mathrm{H}}+1)]$)

$$\mathbf{P}_{1,n}^{\mathrm{T}} = [\mathbf{P}_{1,i}^{\mathrm{T}}, \overbrace{\mathbf{0}_{m(2N_{\mathrm{H}}+1)}^{\mathrm{T}}, \ldots, \mathbf{0}_{m(2N_{\mathrm{H}}+1)}^{\mathrm{T}}}^{(n-1) \text{ times}}] \tag{26}$$

$\mathbf{0}_{m(2N_{\mathrm{H}}+1)}^{\mathrm{T}}$ being the null row of size $m(2N_{\mathrm{H}}+1)$.

4 HB stability assessment of the frequency locked limit cycle

Once the limit cycle has been found by solving the nonlinear algebraic system (24), the Jacobian matrices that give rise to system (4) are also easy to find in terms of their time samples. Notice also that since the most effective numerical solution method of (24) is based on Newton algorithm, such Jacobian matrices are most often already used in the first numerical step.

Time sampling and frequency transforming the governing equation for the Floquet eigenvectors (7), we find the eigenvalue problem of size $nm(2N_{\mathrm{H}}+1)$

$$\left[\tilde{\mathbf{J}}_{\mathbf{f}+\mathbf{g}}(\tilde{\mathbf{x}}_0) - \omega\mathbf{\Omega}_{nm}\right] \tilde{\mathbf{u}}_k = \mu_k \tilde{\mathbf{u}}_k \tag{27}$$

where

$$\begin{aligned}\tilde{\mathbf{J}}_{\mathbf{f}+\mathbf{g}}(\tilde{\mathbf{x}}_0) = \mathbf{\Gamma}_{nm}\, \mathrm{diag}\left\{\hat{\mathbf{J}}_{f_1}(\mathbf{\Gamma}_m^{-1}\tilde{\mathbf{x}}_{10}), \ldots, \hat{\mathbf{J}}_{f_n}(\mathbf{\Gamma}_m^{-1}\tilde{\mathbf{x}}_{n0})\right\} \mathbf{\Gamma}_{nm}^{-1} \\ + \epsilon \begin{bmatrix} \mathbf{\Gamma}_m \hat{\mathbf{J}}_{g_1}(\mathbf{\Gamma}_{nm}^{-1}\tilde{\mathbf{x}}_0)\mathbf{\Gamma}_{nm}^{-1} \\ \vdots \\ \mathbf{\Gamma}_m \hat{\mathbf{J}}_{g_n}(\mathbf{\Gamma}_{nm}^{-1}\tilde{\mathbf{x}}_0)\mathbf{\Gamma}_{nm}^{-1} \end{bmatrix}\end{aligned} \tag{28}$$

Many techniques exist for the efficient solution of the eigenvalue problem (27), see e.g. [36–38]. The numerical algorithms provide a large set of approximations to the Floquet exponents, which as well known are infinite in number since equivalent sets can be defined characterized by imaginary parts differing by an integer multiple of ω [39]. Clearly, the eigenvectors of (27) are the harmonic components of the Floquet eigenvectors of the limit cycle: according to the procedure sketched in [39], they can be used to choose among the various Floquet exponents the ones with minimal numerical error.

5 Example

As an example of application we consider the one-dimensional array of third order oscillators discussed in [8]. Each cell of the array is an instance of the well studied Chua's circuit, that we have chosen because of its wide variety of dynamical behaviors. The cells are coupled by means of a resistive coupling branch, as shown in Fig. 1 where the case of a chain of $N_{\mathrm{cell}} = 3$ oscillators is considered. For the sake of simplicity, we assume nearest neighbors identical coupling among the cells (apart from the first and last cells, coupled to the respective first neighbor only).

By defining a normalized time variable and properly normalized circuit elements, each cell is described by the dimensionless parameters

$$R = 1 \qquad C_2 = 1 \qquad C_1 = \frac{1}{\alpha} \qquad L = \frac{1}{\beta} \tag{29}$$

whereas the nonlinear element is approximated by the cubic dependence

$$i_{\mathrm{C}}(v) = \frac{8}{7}v - \frac{4}{63}v^3 \tag{30}$$

where v is the normalized voltage across C_1. We start our analysis by choosing $\alpha = 8$ and $\beta = 15$, a choice of parameters for which each of the uncoupled cells is characterized by three unstable equilibria (for $v = 0$ and $v = \pm 1.5$),

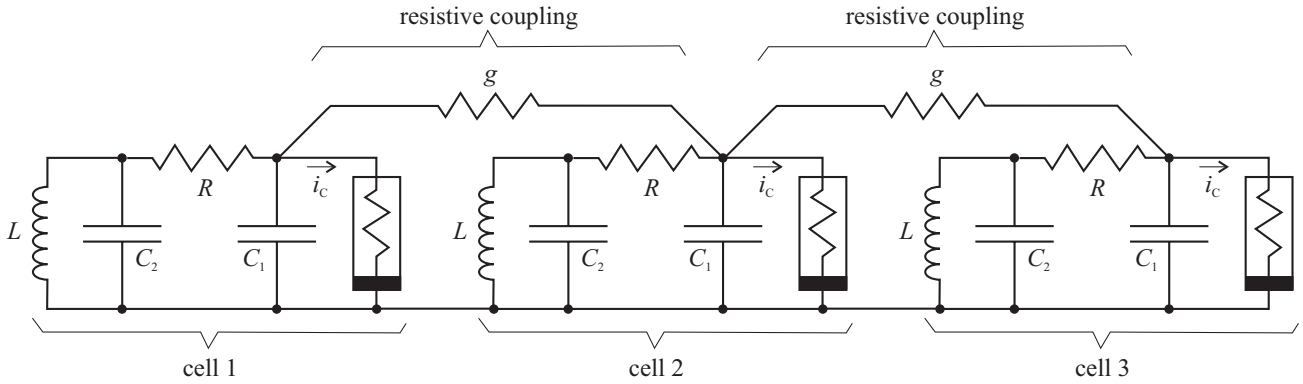

Fig. 1. Example of 3 identical Chua's circuit oscillators connected through a resistive coupling branch among the first neighbours of the chain.

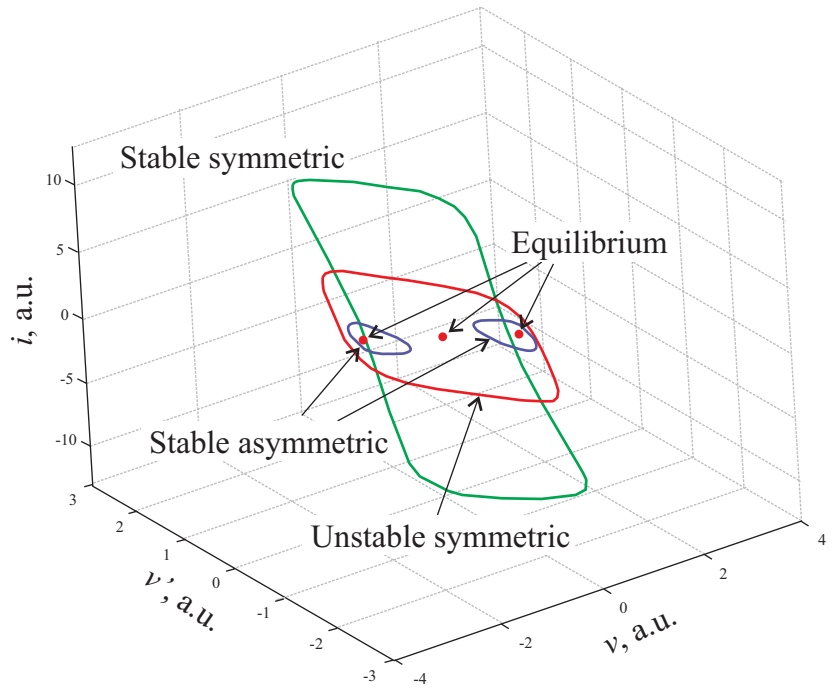

Fig. 2. Equilibra and limit cycles for the uncoupled Chua's circuit with normalized variables and characterized by $\alpha = 8$ and $\beta = 15$. Voltages v and v' are measured on C_1 and C_2, respectively, while i is the current in L.

two asymmetric stable limit cycles, one stable symmetric limit cycle, and one unstable symmetric limit cycle [8, 40] (see Fig. 2). We consider the case of $N_{\text{cell}} = 6$ cells connected by a resistive coupling as shown for 3 cells in Fig. 1.

In the following, all simulations are carried out with our circuit simulator NOSTOS [38, 39], that implements both time- and frequency-domain (HB) solution algorithms for autonomous and forced circuits. Furthermore, the HB evaluation of the Floquet eigenvalues and eigenvectors is also available.

We consider first a time domain simulation (Fig. 3). Starting from a slightly perturbed null initial conditions for the variables (i.e., an unstable equilibrium), the 6 cells coupled with $g = 0.1$ lead to the limit cycle shown in Fig. 3. However, before arriving to the final limit cycle, there are two long transients that can be considered as metastable stationary states, the first one from 0 to 200 time units and the second from 200 to 400 time units. During these two metastable states the system remains very close to an unstable equilibrium (the origin) and an unstable limit cycle (the second interval). In both cases, since they are unstable, a small perturbation is amplified and when sufficiently large it kicks the system far from the metastable solutions. However, since the amplification process is long compared to the intrinsic frequency, the term metastable is justified. Therefore, for this system we have first a metastable equilibrium (time from 0 to 200), then it jumps into a metastable limit cycle (from 200 to 400), then a transient is found (from 400 to 600) and finally it collapses into stable limit cycle.

This time domain analysis represents an interesting case study. In fact, if one uses time domain simulation only, it can be hard to distinguish metastable from stable equilibria or limit cycles, since the perturbation amplification

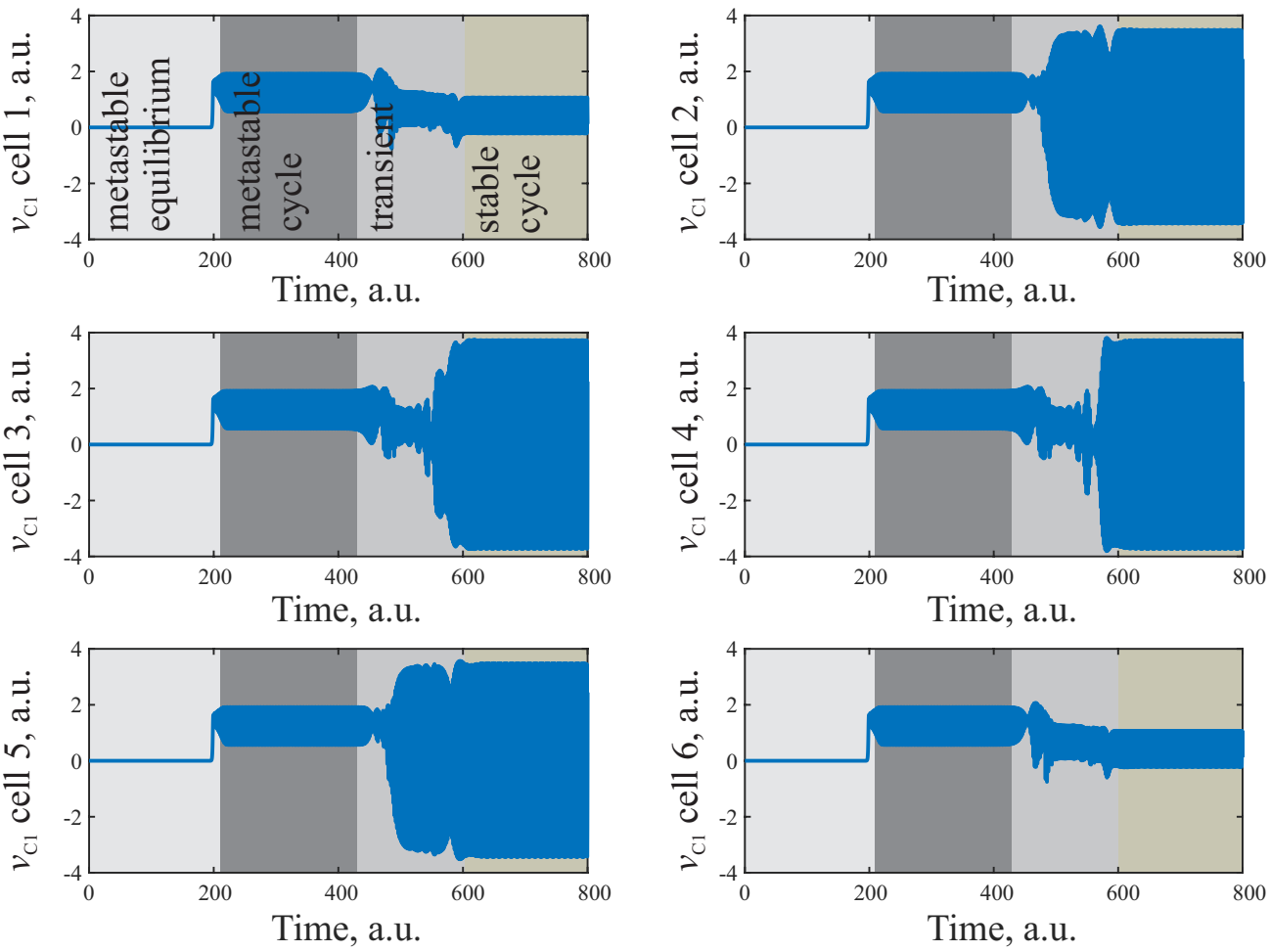

Fig. 3. Time domain simulation of the 6 coupled Chua's circuits ($g = 1.8$). The initial condition is a slightly perturbed zero for all variables that corresponds to a perturbed unstable equilibrium. Here only the voltages on capacitance C_1 for each cell are shown.

process can be very long. On the other hand, using HB stability analysis, we can readily asses if the state is stable or metastable. In the case under study, we concentrate only on the metastable limit cycle between 200 and 400 time units, because the metastable state between 0 and 200 can be studied exploiting the traditional stability analysis for equilibria.

In order to study the metastable limit cycle, we have performed time domain simulation of the system up to 325 time units (see Fig. 4). Then, we have used the last time domain few cycles to derive an initial condition for the solution of nonlinear system (24). An appropriate phase shift has to be enforced in order to minimize the second equation in (24), thus guaranteeing a fast convergence for the HB solution. The HB simulations of the 6 cells coupled circuit have been carried out using $N_{\mathrm{H}} = 20$ harmonics.

Once the HB solution is found, we can perform the stability analysis evaluating the Floquet exponents as discussed in section 4. Fig. 5 demonstrates the numerical evaluation of the eigenvalues of (27). Each Floquet exponent is split into $2N_H + 1$ equivalent Floquet exponents with imaginary parts differing by an integer multiple of ω. However, numerically only the central part of these distributions corresponds to the most accurate multiplier. Notice that these distributions are not always centered around a null imaginary part (purely real Floquet exponent). Therefore, we have implemented in NOSTOS an advanced numerical method based on clustering using a definition of distance involving both Flouet eigenvalues and eigenvectors. This method allows us to select at the same time the different distributions and their central estimates of the Floquet exponents guaranteeing a high accuracy (see Fig. 5).

From the zoomed plot in Fig. 5, we can recognize that the limit cycle we are considering is actually unstable (as predicted by the long time domain simulation) with 8 unstable manifolds. Due to the complexity of the system, it is not easy to classify these manifolds and an exhaustive analysis would be out of the scope of this work.

Once the stability of this limit cycle has been assessed, we seek whether values of circuit parameters such as the coupling strength (g) or the α coefficient make the limit cycle stable. To this end, we have performed a parameter

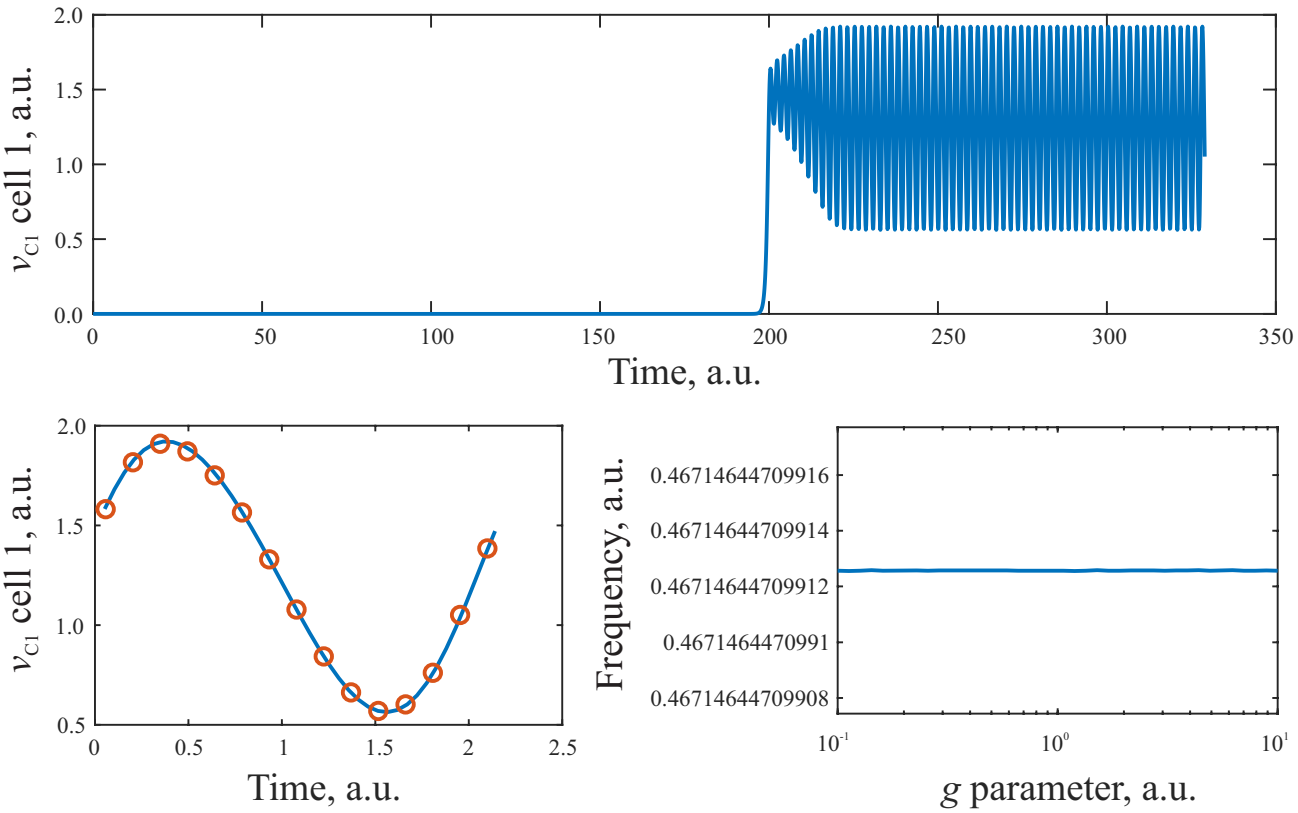

Fig. 4. Time domain simulation of the 6 coupled Chua's circuits. Even changing g over two orders of magnitude (from 0.1 to 10), the limit cycle is unchanged, with a constant frequency (lower right figure). In the lower left figure, the HB solution of $V_{C_1}(t)$ is shown over one period for $g = 0.1$ (line) and $g = 10$ (symbols) (obtained employing a continuation algorithm from $g = 0.1$ to $g = 10$ in 50 points logarithmically spaced), showing that the two waveforms and frequencies are identical.

sweeping in both g and α, exploiting a sophisticated continuation algorithm [23] implemented in NOSTOS for both limit cycles and Floquet exponents. We have initially varied g from $g = 0.1$ to $g = 10$ in a logarithmically spaced selection of values. From Fig. 4 we can see that both the limit cycle and its frequency are independent of g. In fact, the coupling only locks the oscillators and if they are assuming identical in phase oscillations no current flows through g. However, as shown in Fig. 6, increasing g the unstable manifolds become stable one after the other: for $g \approx 2$ the last unstable manifold disappears and the limit cycle undergoes a bifurcation becoming stable. Notice the presence of the null Floquet exponent, always present when an autonomous system admits of a non trivial limit cycle.

Another interesting stability analysis for the system can be carried out by varying α. In this case, we have reduced α from 8 to 6 in linearly spaced values while keeping $g = 1.8$. From Fig. 7 we can see that frequency increases and the amplitude of the cycle shrinks: for $\alpha \approx 7$ the limit cycle disappears and collapses into an equilibrium. Looking at the α dependence of the Floquet eigenvalues closer to a zero real part in Fig. 8, we can see that for $\alpha = 8$ the limit cycle is unstable, with a first bifurcation at about $\alpha \approx 7.7$ where the cycle becomes stable. Finally, another bifurcation takes place at $\alpha \approx 7$, below which the cycle collapses into a stable equilibrium. Notice that the null FE disappears when the limit cycle collapses into an equilibrium.

6 Conclusion

We have discussed in detail an algorithm for the determination of the limit cycle of autonomous nonlinear oscillators in the frequency domain by means of an efficient implementation of the Harmonic Balance technique. Frequency locking among coupled oscillators is also studied in the frequency domain by means of a properly devised HB algorithm, and by proposing a technique for the determination of the Floquet eigenvalues and eigenvectors of the above mentioned limit cycle.

The proposed algorithms, implemented into an in house circuit simulator, were used to study the frequency locking of a set of Chua's oscillators coupled by means of a resistive element connecting the first neighbor cells. The results demonstrate the capabilities of HB for the parametric analysis of the frequency locked limit cycle stability.

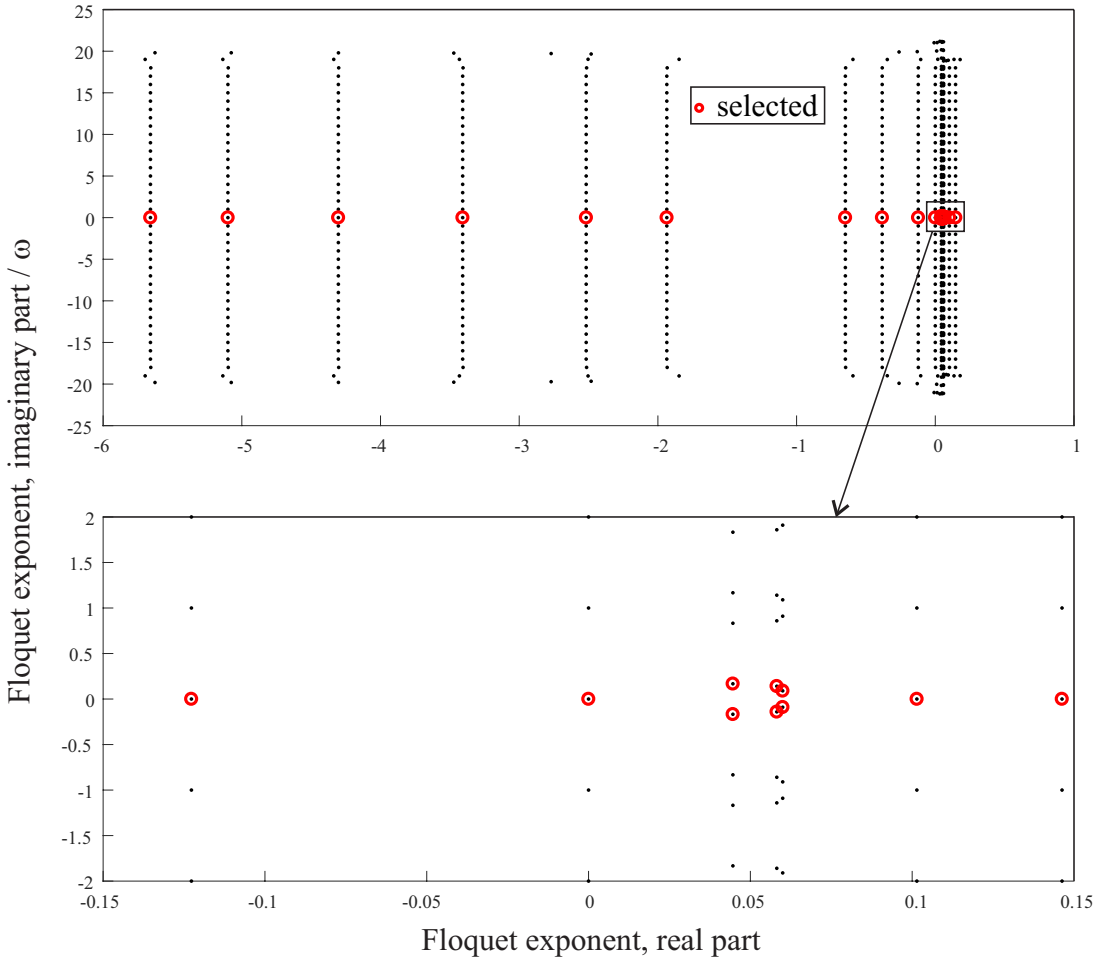

Fig. 5. Floquet exponents in the complex plane for the limit cycle computed form $\alpha = 8$ and $g = 0.1$. The red symbols denotes the FEs determined by the choice algorithm exploiting the Floquet eigenvectors.

References

1. A. Pikovsky, M. Rosenblum, J. Kurths, *Synchronization: a universal concept in nonlinear sciences*, vol. 12 (Cambridge university press, 2003)
2. G.V. Osipov, J. Kurths, C. Zhou, *Synchronization in oscillatory networks* (Springer Science & Business Media, 2007)
3. C.S. Peskin, *Mathematical aspects of heart physiology* (Courant Institute of Mathematical Sciences, New York University, 1975)
4. C. Liu, D.R. Weaver, S.H. Strogatz, S.M. Reppert, Cell **91**(6), 855 (1997). DOI 10.1016/S0092-8674(00)80473-0
5. H.G. Winful, L. Rahman, Physical Review Letters **65**(13), 1575 (1990). DOI 10.1103/PhysRevLett.65.1575
6. R. Roy, K.S. Thornburg Jr, Physical Review Letters **72**(13), 2009 (1994). DOI 10.1103/PhysRevLett.72.2009
7. R.A. York, R.C. Compton, IEEE Trans. Microw. Theory Tech. **39**(6), 1000 (1991). DOI 10.1109/22.81670
8. M. Bonnin, F. Corinto, M. Gilli, IEEE Trans. Circuits Syst. I, Regul. Pap. **55**(6), 1671 (2008). DOI 10.1109/TCSI.2008.916460
9. E.T. Hall, *The dance of life: The other dimension of time* (Anchor, 1984)
10. A.T. Winfree, Journal of theoretical biology **16**(1), 15 (1967). DOI 10.1016/0022-5193(67)90051-3
11. R. MacKay, S. Aubry, Nonlinearity **7**(6), 1623 (1994). DOI 10.1088/0951-7715/7/6/006
12. S.I. Shima, Y. Kuramoto, Physical Review E **69**(3), 036213 (2004). DOI 10.1103/PhysRevE.69.036213
13. M. Bonnin, Physica D: Nonlinear Phenomena **238**(1), 77 (2009). DOI 10.1016/j.physd.2008.08.015
14. K.R. Crounse, L.O. Chua, IEEE Transactions on Circuits and Systems I: Fundamental Theory and Applications **42**(10), 583 (1995). DOI 10.1109/81.473566
15. L. Goras, L.O. Chua, IEEE Transactions on Circuits and Systems I: Fundamental Theory and Applications **42**(10), 612 (1995). DOI 10.1109/81.473568
16. P. Thiran, G. Setti, M. Hasler, IEEE Transactions on Circuits and Systems I: Fundamental Theory and Applications **45**(8), 777 (1998). DOI 10.1109/81.704819

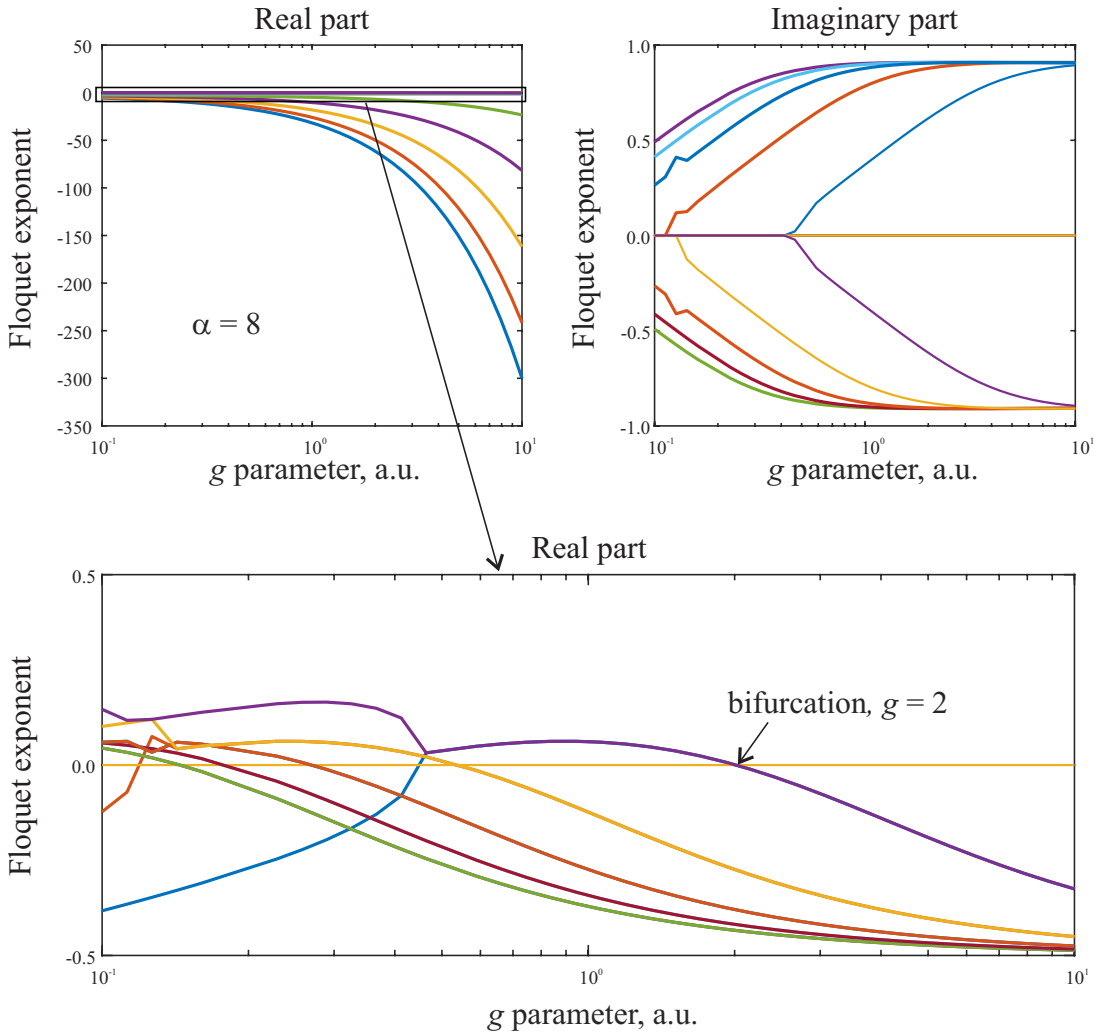

Fig. 6. Real and imaginary parts of the Floquet exponents as a function of g for $\alpha = 8$.

17. G. Setti, P. Thiran, C. Serpico, IEEE Transactions on Circuits and Systems I: Fundamental Theory and Applications **45**(8), 790 (1998). DOI 10.1109/81.704820
18. M. Bonnin, M. Gilli, P.P. Civalleri, IEEE Transactions on Circuits and Systems II: Express Briefs **52**(9), 525 (2005). DOI 10.1109/TCSII.2005.850518
19. F.L. Traversa, F. Bonani, S. Donati Guerrieri, Int. J. Circuit Theory Appl. **36**(4), 421 (2008). DOI 10.1002/cta.440
20. J.K. Hale, S.M. Verduyn Lunel, *Introduction to functional-differential equations*, *Applied Mathematical Sciences*, vol. 99 (Springer-Verlag, New York, 1993)
21. N. MacDonald, J. Sound Vib. **186**(4), 649 (1995). DOI 10.1006/jsvi.1995.0475
22. F. Cappelluti, F.L. Traversa, F. Bonani, S. Donati Guerrieri, G. Ghione, IEEE Microw. Guided Wave Lett. **24**(7), 493 (2014). DOI 10.1109/LMWC.2014.2316236
23. F.L. Traversa, F. Bonani, F. Cappelluti, in *2013 IEEE MTT-S International Microwave Symposium Digest (MTT)* (IEEE, 2013). DOI 10.1109/mwsym.2013.6697643
24. F. Traversa, M. Di Ventra, F. Cappelluti, F. Bonani, ArXiv e-prints (2013). URL https://arxiv.org/abs/1308.3796v1
25. A. Maritan, J.R. Banavar, Phys. Rev. Lett. **72**, 1451 (1994). DOI 10.1103/PhysRevLett.72.1451
26. A. Neiman, L. Schimansky-Geier, A. Cornell-Bell, F. Moss, Phys. Rev. Lett. **83**, 4896 (1999). DOI 10.1103/PhysRevLett.83.4896
27. B. Øksendal, *Stochastic Differential Equations*, 6$^{\text{th}}$ edn. (Springer-Verlag Berlin Heidelberg, 2003). DOI 10.1007/978-3-642-14394-6
28. M. Bonnin, F.L. Traversa, F. Bonani, IEEE Trans. Circuits Syst. Express Briefs **63**(7), 698 (2016). DOI 10.1109/TCSII.2016.2532098
29. M. Bonnin, Int. J. Circuit Theory Appl. **45**(5), 636 (2017). DOI 10.1002/cta.2246
30. M. Bonnin, F. Corinto, V. Lanza, Eur. Phys. J. Spec. Top. **225**, 171 (2016). DOI 10.1140/epjst/e2016-02617-8
31. M. Farkas, *Periodic motions* (Springer-Verlag, New York, 1994)

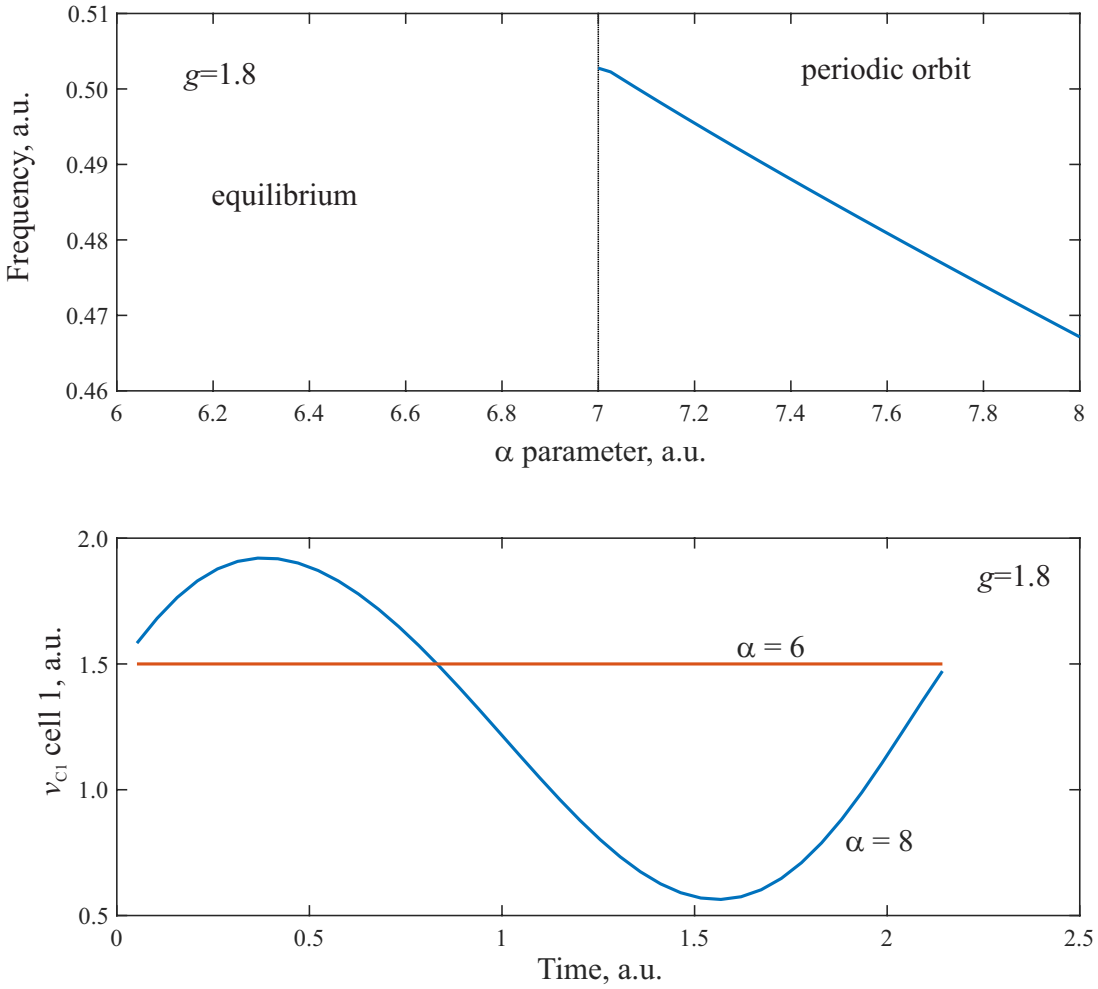

Fig. 7. Dependence on parameter α of the oscillation frequency (top figure) and time dependence of the voltage across C_1 for a circuit made of 6 identical cells with $g = 1.8$. Reducing α starting from $\alpha = 8$ corresponds initially to a limit cycle, while for $\alpha \leq 7$ the solution collapses into an equilibrium.

32. F.L. Traversa, M. Di Ventra, F. Bonani, Phys. Rev. Lett. **110**(17), 170602 (2013). DOI 10.1103/PhysRevLett.110.170602
33. F. Bonani, F. Cappelluti, S. Donati Guerrieri, F. Traversa, *Harmonic Balance Simulation and Analysis* (John Wiley & Sons, 2014). DOI 10.1002/047134608X.W8210
34. K. Kundert, A. Sangiovanni-Vincentelli, J. White, *Steady-state methods for simulating analog and microwave circuits* (Kluwer Academic Publisher, Boston, 1990)
35. B. Troyanovsky, Frequency domain algorithms for simulating large signal distorsion in semiconductor devices. Ph.D. thesis, Stanford Univ., Stanford, CA (1997)
36. F.L. Traversa, F. Bonani, IET Circuits Devices Syst. **5**(1), 46 (2011). DOI 10.1049/iet-cds.2010.0138
37. F.L. Traversa, F. Bonani, AEÜ - International Journal of Electronics and Communications **66**(5), 357 (2012). DOI 10.1016/j.aeue.2011.09.002
38. F.L. Traversa, F. Bonani, IEEE Trans. Computer-Aided Design Integr. Circuits Syst. **32**(2), 313 (2013). DOI 10.1109/TCAD.2012.2214480
39. F. Cappelluti, F.L. Traversa, F. Bonani, S. Donati Guerrieri, G. Ghione, IEEE Trans. Microw. Theory Tech. **61**(4), 1580 (2013). DOI 10.1109/TMTT.2013.2248017
40. A.I. Khibnik, D. Roose, L.O. Chua, Int. J. Bifurcation Chaos Appl. Sci. Eng. **3**(2), 363 (1993). DOI 10.1142/S021812749300026X

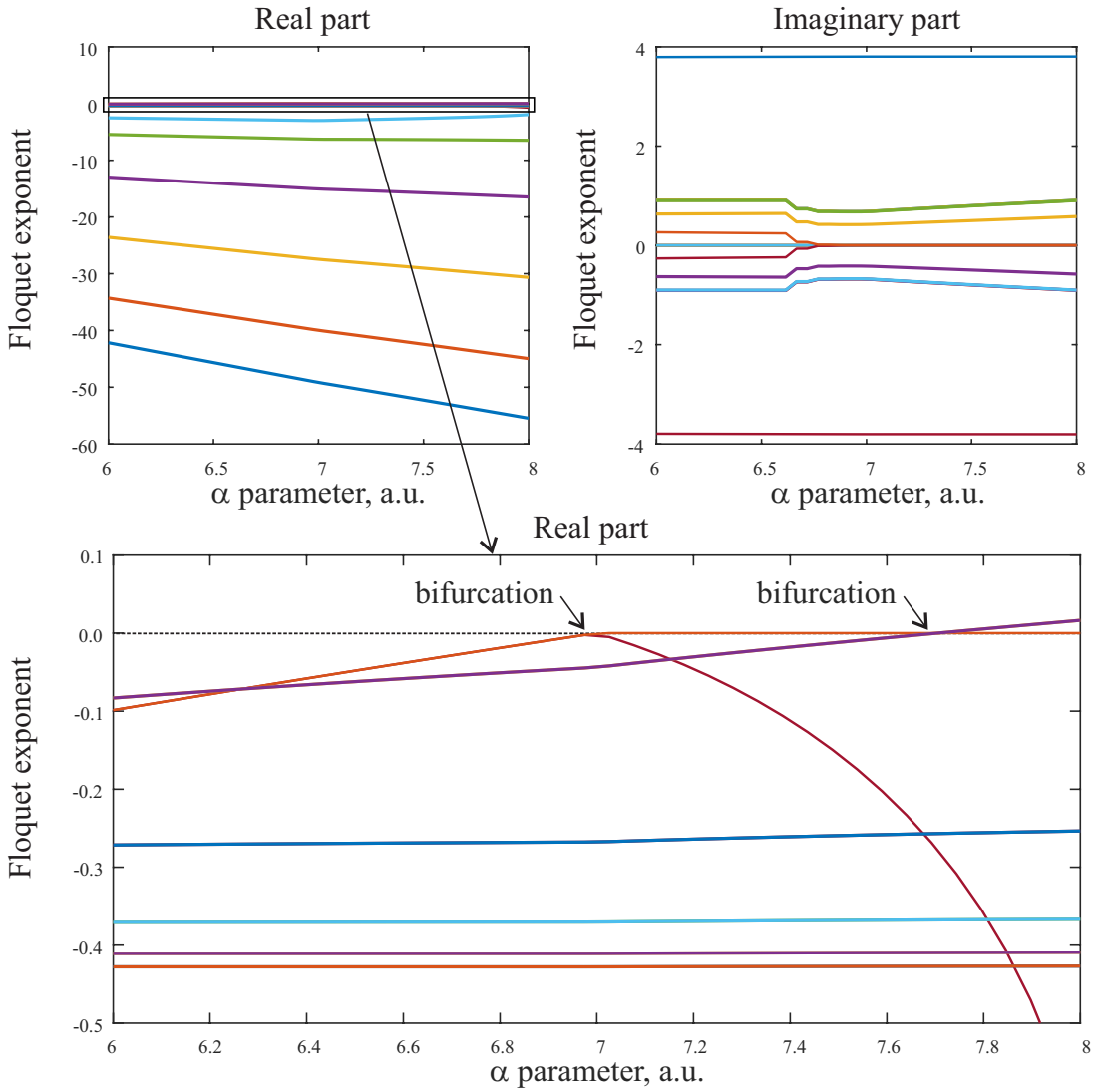

Fig. 8. Real and imaginary parts of the Floquet exponents as a function of α for $g = 1.8$.